Pflugers Arch - Eur J Physiol (2009) 458:273–281
DOI 10.1007/s00424-008-0617-z

ION CHANNELS, RECEPTORS AND TRANSPORTERS

Pairwise coupling of hair cell transducer channels links auditory sensitivity and dynamic range

Sietse M. van Netten · Cécil J. W. Meulenberg · George W. T. Lennan · Corné J. Kros

Received: 21 August 2008 / Accepted: 4 November 2008 / Published online: 2 December 2008

Abstract Hair cells in the inner ear provide the basis for the exquisite hearing capabilities of mammals. These cells transduce sound-induced displacements of their mechanosensitive hair bundle into electrical currents within a fraction of a millisecond and with nanometer fidelity. Excitatory displacements of the hair cell's bundle tense tip links that open transducer channels. These channels are located either at one or at both ends of the links, where the latter possibility was thought to compromise sensitivity via negative cooperativity, and discarded for quantitatively describing the transduction process. Here, we show instead that this series mode of activation accurately explains measured transduction in hair cells. It enhances both sensitivity and dynamic range of hair cell transduction, by one channel that is extremely sensitive at small displacements while the other responds best to larger stimuli. Our results provide a new framework for exploring the dynamics of hair cell activation.

S. M. van Netten (✉) · C. J. W. Meulenberg
Department of Neurobiophysics,
University of Groningen,
Nijenborgh 4,
9747 AG Groningen, The Netherlands
e-mail: s.m.van.netten@rug.nl

S. M. van Netten
Artificial Intelligence and Cognitive Engineering,
University of Groningen,
Nijenborgh 9,
9747 AG Groningen, The Netherlands

C. J. W. Meulenberg · G. W. T. Lennan · C. J. Kros
School of Life Sciences, University of Sussex,
Falmer,
Brighton BN1 9QG, UK

Keywords Hair cell · Transduction · Mechanoreceptor · Ion channel · Hearing · Mechanosensitive channel · Mechano-electrical transduction

Introduction

The identities and precise activation mechanisms of molecules that transfer hair bundle displacement into ionic transducer currents remain to be established [1–3]. Yet, many properties of transducer channel activation observed across several different hair cell types are consistent with the gating-spring model [4–7]. This thermodynamics-based model explains channel activation by assuming that excitatory bundle displacement tenses elastic elements, termed gating springs, that force the gates of the channels into their open conformational state. The location of the transducer channels has been experimentally determined to be close to the tips of the stereocilia [8, 9]. Prominent structures in this region of the hair bundle are tip link filaments [10, 11], without which there is no transduction [12]. A tip link runs upward from the vertex of a stereocilium towards the side of an adjacent taller stereocilium (Fig. 1a). Tip links will be tensed when the hair bundle is pushed toward the taller stereocilia [1, 10], coincident with the observed directional sensitivity of hair cells [13]. Although probably not constituting the gating springs themselves [14], tip links are now widely believed to be involved in tensing the gating springs.

Reports on the number of transducer channels engaged by a single tip link diverge between one and two [4, 15–17]. However, so far, gating-spring models quantifying channel open probability assume each tip link to activate a single channel. Here, we quantify for the first time mechano-electrical transduction mediated by pairs of transducer channels, mechanically in series via gating springs at both

ends of one tip link (Fig. 1b). This series mode of engagement not only accurately explains transduction in a variety of hair cell types but also reveals a novel and unexpected consequence of having two geometrically arranged groups of transducer channels. It enhances both sensitivity and dynamic range of hair cell transduction, by having one channel possessing high sensitivity over a narrow range of small stimulus levels and a second one encoding mainly larger stimuli.

Materials and methods

Schematics of the model, in which a single tip link engages two channels, are shown in Fig. 1. The model's mode of engagement is in line with previous measurements that indicate the presence of transducer channels on either side of a tip link [15]. The model is also supported by a detailed analysis of transducer conductance per tip link revealing a maximum of two operational transducer channels per tip link [17].

The equilibrium open probability of a transducer channel pair versus hair bundle displacement, or activation curve, of this scheme of transducer channel activation is derived below.

Geometry of the model

The geometry of the model is illustrated in Fig. 1b, where a single tip link (magenta) is mechanically in series with two transducer channels (green), which are also each in series with a gating spring (red). The gating springs are anchored on actin filaments via one (cf. Fig. 1b) or possibly two (not shown) myosin motors (blue) [cf. 18, 19]. The two elastic gating springs in series, with stiffness k_1 and k_2 (Fig. 1b), are mechanically equivalent to one gating spring with stiffness $k_s = k_1 k_2/(k_1 + k_2)$ (Fig. 1c). When the two channels each have dual-conformational-state kinetics and the related conformational swing distances between their open (O) and closed (C) states are d_1 and d_2, the gating forces sensed at the molecular level of the two channels are defined by $z_1 = k_s d_1$ and $z_2 = k_s d_2$, respectively.

Open probability

The four possible combinations of the two conformational states of the two channels are labeled with two indices i, j denoting the state of respectively population (1) and (2), which can be either open (O) or closed (C) (see Fig. 1c). The (Helmholtz) free energy, E_{ij}, of each of these four combinations consists of the sum of a component, μ_{ij}, representing the intrinsic conformational energy of the two channels under conditions of a relaxed gating spring, and a component that depends on the extension and related potential energy of the gating spring, which is assumed to be Hookean. The extension of each gating spring, x, is assumed to be linearly related to the deflection of the hair

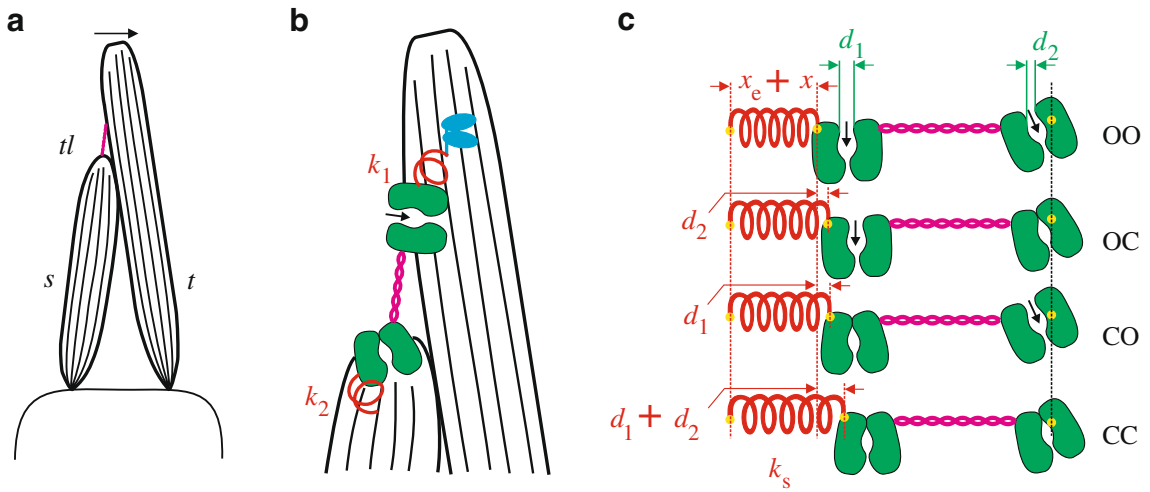

Fig. 1 Series engagement of two hair cell transducer channels by a single tip link (*magenta*). **a** Mechanical stimulation of a hair bundle into the excitatory direction (*arrow*) causes rigid stereocilia, containing actin filaments (*black lines*), to pivot around their insertion points in the apical plate so that tip links (*tl*) running from shorter stereocilia (*s*) towards the tips of taller (*t*) ones are tensed. **b** Tension in a single tip link engages two transducer channels (*green*) at both ends of the tip link. Both channels are in series with a gating spring (*red*) which have stiffness k_1 and k_2, respectively. Pre-tensing may occur via myosin motor proteins (*blue*) that produce forces via their interaction with actin. **c** The two gating springs in series are equivalent to an effective spring (stiffness k_s), which is stretched depending on the conformational state of the two channels that have swing distances d_1 and d_2. If each channel has an open (O) and a closed (C) state, for a channel pair effectively four different combinations result (*OO* both channels open, *OC* channel (1) open and channel (2) closed, *CO* channel (1) closed and channel (2) open, *CC* both channels closed), so that the total extension of the effective spring consists of a sum of respectively 0, d_2, d_1, or d_1+d_2 and a pre-extension, x_e, plus an amount x, which depends linearly on hair bundle displacement (X). Via the related free energies of the four combinations, and using Boltzmann statistics, the open probabilities are defined (Eq. 1)

bundle, X, both referenced to the resting position of the hair bundle. It is further assumed that a gating spring has a pre-tension associated with an elongation x_e at rest (i.e., at $x=0$), most likely effected by a myosin motor. Depending on the combination of conformational states (OO, OC, CO, or CC), an extra extension of the gating spring of respectively 0, d_2, d_1, or d_1+d_2 is present (Fig. 1c). Together, this yields the free energies, $E_{OO} = \mu_{OO} + \frac{1}{2}k_s(x_e + x)^2$, $E_{OC} = \mu_{OC} + \frac{1}{2}k_s(x_e + x + d_2)^2$, $E_{CO} = \mu_{CO} + \frac{1}{2}k_s(x_e + x + d_1)^2$ and $E_{CC} = \mu_{CC} + \frac{1}{2}k_s(x_e + x + d_1 + d_2)^2$. From these energies, the probabilities of the four combinations, p_{ij}, are determined via Boltzmann statistics:

$$p_{ij} \propto \exp\left(-E_{ij}/kT\right), \quad i,j \in \{O, C\}, \tag{1}$$

where k is Boltzmann's constant and T the absolute temperature. The open probability of channel population (1), p_1, is then given by:

$$p_1 = (p_{OO} + p_{OC})(p_{OO} + p_{OC} + p_{CO} + p_{CC})^{-1}, \tag{2}$$

while the open probability of population (2), p_2, is:

$$p_2 = (p_{OO} + p_{CO})(p_{OO} + p_{OC} + p_{CO} + p_{CC})^{-1}. \tag{3}$$

Transforming from molecular variables (lower case) to those as sensed at the hair bundle's tip (upper case), so that for instance distance, x, and force, z, correspond to X and Z, it is noted that energies, and therefore products of distance and force, are invariant under this transformation (cf. $x \cdot z = X \cdot Z$).

For a hair bundle displacement, X, the equilibrium open probability or activation curve of a channel pair, $p(X)$, assuming identical conductance of the two channels, then consists of the contributions of the two companion channels, $p_1(X)$ and $p_2(X)$:

$$p(X) = [p_1(X) + p_2(X)]/2. \tag{4}$$

The open probabilities of the two populations, p_1 and p_2 (Eqs. (2) and (3)) can be rewritten with Eq. (1), and using $x \cdot z = X \cdot Z$, as:

$$p_1(X) = [1 + K_2 \exp(-Z_2\,\Delta X/kT)]/H(X), \tag{5}$$

$$p_2(X) = [1 + K_1 \exp(-Z_1\,\Delta X/kT)]/H(X), \tag{6}$$

where H is a normalized partition function:

$$\begin{aligned} H(X) = {} & 1 + K_1 \exp(-Z_1\,\Delta X/kT) \\ & + K_2 \exp(-Z_2\,\Delta X/kT) \\ & + \exp[-(Z_1 + Z_2)\,\Delta X/kT], \end{aligned} \tag{7}$$

and with

$$\Delta X = X - X_0. \tag{8}$$

Here, Z_1 and Z_2 are the gating forces (cf. z_1, z_2) as sensed at the hair bundle's tip, while they also characterize the two channels' intrinsic displacement sensitivities while X_0 is a set point where half the conductance is activated ($p(X_0)=0.5$), which depends on the sensitivities, the differences of energies of unengaged closed- and open-channel states, μ_{CC}–μ_{OO}, the effective conformational swings (D_1 and D_2), and the pre-extension (X_e) as felt at the hair bundle's tip (cf. Fig. 1c) according to:

$$X_0 = -\frac{D_1 + D_2}{2} - X_e - \frac{\mu_{CC} - \mu_{OO}}{Z_1 + Z_2}. \tag{9}$$

The dimensionless (positive) interaction parameters K_1 and K_2 govern the interaction between the two channels (see "Results" section) and depend on the unengaged free energies of the open and closed configurations of the two channels μ_{ij}, and the pre-extension X_e. The interaction parameters also relate straightforwardly to the individual set points (X_{01} and X_{02}) of the two subpopulations (see Eqs. (11) and (12)). These individual set points also bear a useful relationship to the physical parameters of the model (see Eqs. (12) and (14)).

The transducer conductance of a hair cell, G, is proportional to the open probability (Eq. (4)) via:

$$G(X) = G_T p(X), \tag{10}$$

where G_T is the hair cell's maximum transducer conductance.

Interdependency of channel pair

The interaction parameters (K_1, K_2) are related to the individual set points of the two channels (see also "Results" section). If the product of K_1 and K_2 is unity ($K_1 \cdot K_2 = 1$), interaction appears to be completely absent, so that the channels are effectively independently engaged and the model reduces to that of two independently activated channels. This can be seen by multiplying nominator and denominator of Eqs. (5) and (6) by $1 + K_1 \exp(-Z_1\,\Delta X/kT)$ and $1 + K_2 \exp(-Z_2\,\Delta X/kT)$, respectively. Then p_1 and p_2 reduce to first-order Boltzmann functions with displacement sensitivities Z_1 and Z_2, and with individual set points, X_{01} and X_{02}:

$$p_1(X) = [1 + \exp\left(-Z_1(X - X_{01})/kT\right)]^{-1}, \text{ with}$$

$$X_{01} = X_0 + \frac{kT}{Z_1}\ln K_1 = X_0 - \frac{kT}{Z_1}\ln K_2, \tag{11}$$

and

$$p_2(X) = [1 + \exp(-Z_2(X - X_{02})/kT)]^{-1}, \text{ with}$$

$$X_{02} = X_0 + \frac{kT}{Z_2}\ln K_2. \tag{12}$$

While the condition of full independency ($K_1 \cdot K_2 = 1$) is not completely met, we find for OHCs, VHCs, and other hair

cell types that $K_1<1$ and $K_2>1$ (see "Results" section), and that the measurements are very well approximated by the set points X_{01} and X_{02}, given in Eqs. (11) and (12). Since $K_2>1$, the most sensitive population (1) has its set point (X_{01}) to the left of X_0 (Eq. 11), while the less sensitive population (2) has its set point (X_{02}) to the right of X_0 (Eq. 12).

Expressions of these set points in terms of the physical parameters of the model are:

$$X_{01} = -\frac{D_1}{2} - X_e - \frac{\mu_{CO} - \mu_{OO}}{Z_1}, \quad (13)$$

and

$$X_{02} = -\frac{D_2}{2} - X_e - \frac{\mu_{OC} - \mu_{OO}}{Z_2}. \quad (14)$$

Recording of transducer currents from mouse hair cells

The series engagement model was tested on a set of transducer conductance data of mouse hair cells [20] obtained from simultaneous measurements, just after the onset of force steps, of transducer current at a holding potential of −84 mV and the position of the hair bundle, which was stimulated with a fluid jet. Additional data from four outer hair cells from which transducer currents and bundle displacements were recorded both at −84 mV and at +86 mV were included to test the effects of depolarization to near the Ca^{2+} equilibrium potential. For the latter experiments, patch pipettes contained (mM) 135 CsCl, 0.1 $CaCl_2$, 5 EGTA–NaOH, 3.5 $MgCl_2$, 2.5 Na_2ATP, and 5 HEPES–NaOH, at a pH of 7.3. Otherwise, methods were as reported before [20].

Fitting procedure

Fits of model equations to measured data were made using the nonlinear least squares fitter of Origin (Microcal Software Inc., Northampton, MA, USA).

Results

Figure 2 shows two examples of transducer conductance (squares), measured at a holding potential of −84 mV as a function of hair bundle displacement in mouse cochlear outer hair cells (OHC, Fig. 2a) and mouse vestibular hair cells (VHC, Fig. 2b).

Gating forces, set points, and conductance

Fitting the model's predicted transducer conductance (Eq. 10, cf. Fig. 2, red curves) to the measurements yielded quantitative values of the two gating forces Z_1, Z_2, which appeared to be different, the overall set point X_0, the interaction parameters K_1, K_2, and the maximum transducer conductance G_T (see "Materials and methods" section). We found that all data sets [20] of both VHC- and OHC-transducer conductance-displacement measurements are

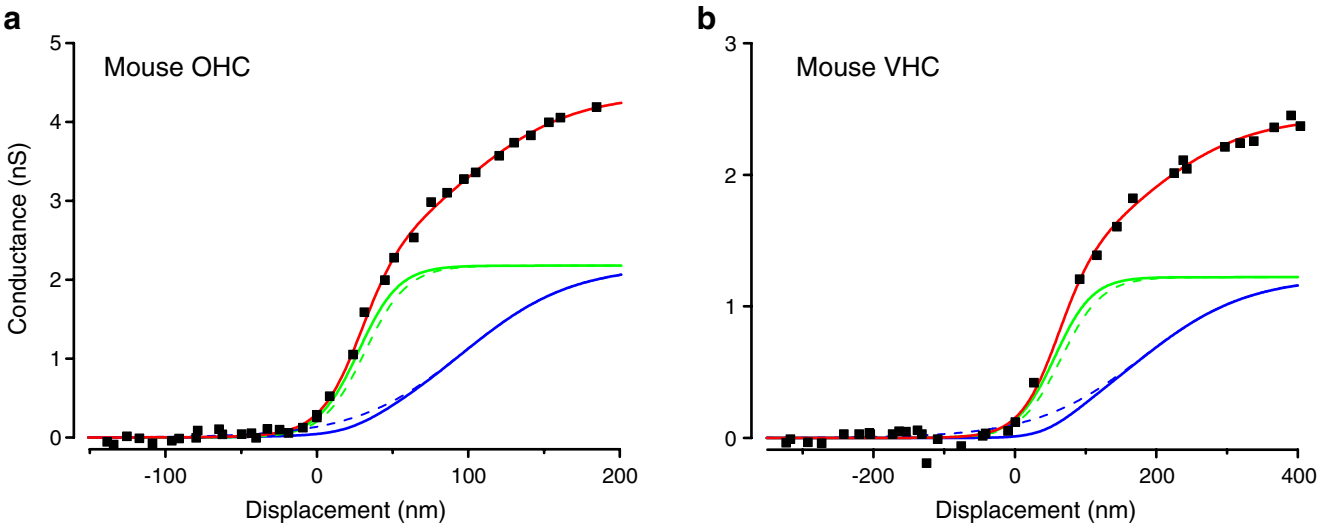

Fig. 2 Measured transducer conductance in mammalian hair cells, compared with model calculations of two transducer channels engaged in series by a single tip link. *Red curves* show model responses (Eqs. 1–10) fitted to the total activated conductance (*squares*), while the *solid green and blue curves* depict individual contributions of the two populations of channels (Eqs. 5–8). *Dashed lines* show contributions of the two populations under conditions of independent engagement via the series spring (Eqs. 11 and 12; first-order Boltzmann functions with sensitivity values Z_1 and Z_2 as obtained from fits). **a** Transducer conductance in a mouse outer hair cell (*OHC*). Fitted parameters: Z_1=294 fN; Z_2=114 fN; X_0=48 nm; K_1=0.058; K_2=3.95; G_T=4.36 nS. **b** Transducer conductance in a mouse vestibular hair cell (*VHC*). Fitted parameters: Z_1=144 fN; Z_2=54 fN; X_0=94 nm; K_1=0; K_2=3.13; G_T=2.44 nS. Holding potential −84 mV

very accurately described by the series engagement model (R^2 range=0.992–0.999; mean=0.99709; n=13).

The individual contributions of the two channel populations follow from the fitted parameters (cf. Fig. 2, solid green and blue curves) and inserting them in Eqs. (5)–(8). In OHCs, the most displacement-sensitive channel population (1) has a gating force Z_1=386±84 fN (mean±s.e.; n=8), and is halfway activated at X_{01}=29±4 nm ($p_1(X_{01})$=0.5; cf. Fig. 2a, solid green curve). The less displacement-sensitive channel population (2) has a concurrent smaller gating force Z_2=162±31 fN and is halfway activated at X_{02}=94±11 nm (cf. Fig. 2a, solid blue curve). Similarly, discernable contributions of two channels to the overall transducer conductance were found for VHCs (Fig. 2b): Z_1=149±49 fN and X_{01}=82±22 nm; Z_2=99±44 fN and X_{02}=171±36 nm (mean±s.e.; n=5). For OHCs, the overall set point is X_0=49±7 nm, and the maximum conductance G_T=5.4±0.5 nS, while for VHCs these values are X_0=113±22 nm and G_T=2.2±0.4 nS (cf. [20]).

As shown in Fig. 3, our results on mouse OHCs and VHCs are supported by excellent fits of the model (Eqs. 1–8) to transducer activation data reported for turtle auditory [21] as well as frog saccular [22] and rat cochlear hair cells [17], which all showed similar contributions of channel activation of the two populations to those found in mouse OHCs and VHCs.

Interdependency of channel engagement

It appears (see "Materials and methods" section) that the two interaction parameters, K_1 and K_2, govern the interdependency of the two channels. For OHCs, the fits yielded

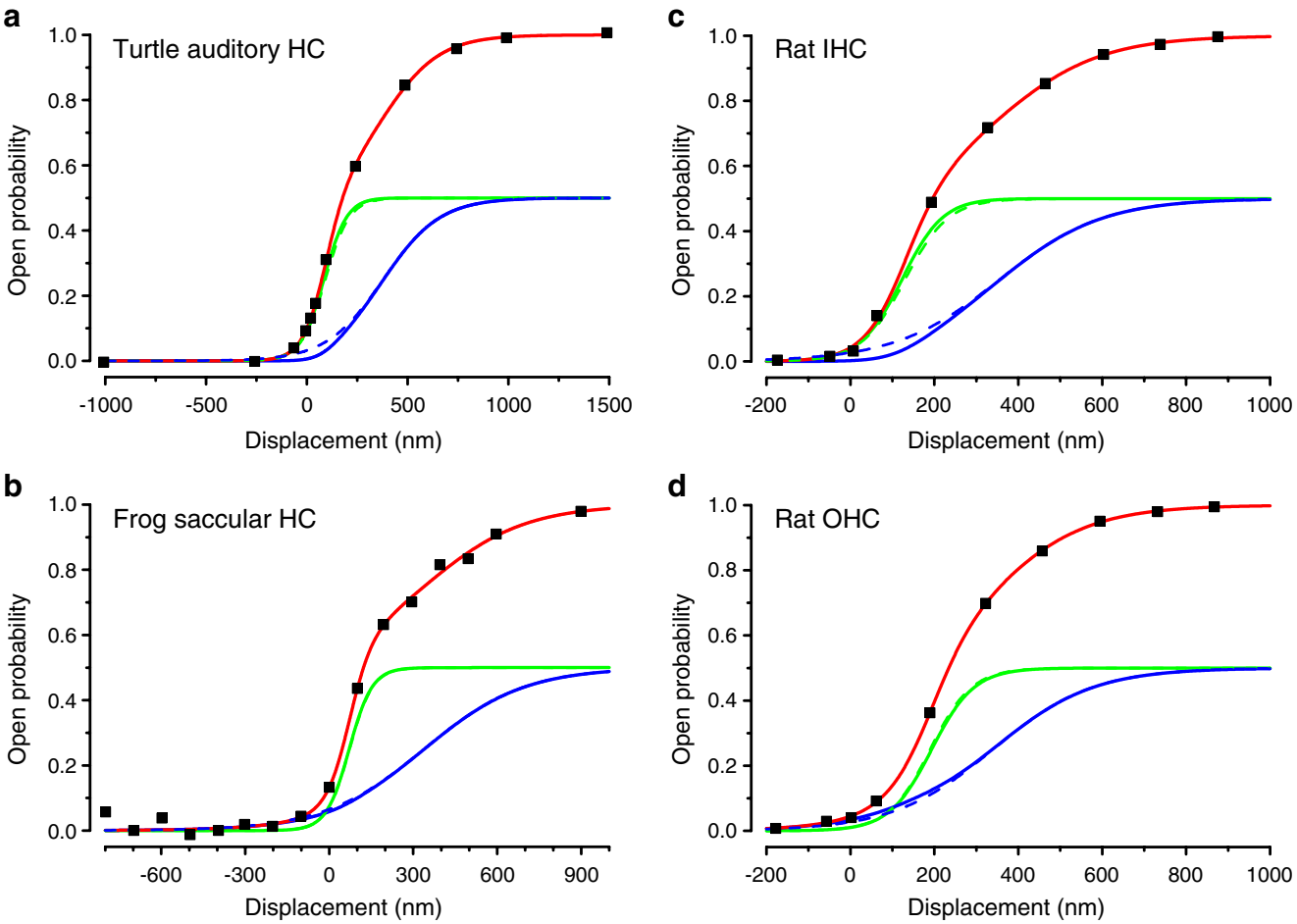

Fig. 3 Fits of the series engagement model to measurements of transducer activity in various hair cell types taken from literature. **a** Turtle auditory hair cell (data from figure 2 of [21]). Fitted parameters: Z_1=68 fN; Z_2=29 fN; X_0=177 nm; K_1=0; K_2=4.18. **b** Frog saccular hair cell (data were taken from figure 8f of [23]). Fitted parameters: Z_1=100 fN; Z_2=23 fN; X_0=122 nm; K_1=0.25; K_2=3.36. **c** Rat inner hair cell (data were taken from figure 2c of [17]). Fitted parameters: Z_1=79 fN; Z_2=33 fN; X_0=196 nm; K_1=0; K_2=3.58. **d** Rat outer hair cell (data were taken from figure 2a of [17]). Fitted parameters: Z_1=83 fN; Z_2=34 fN; X_0=234 nm; K_1=0.53; K_2=2.43. *Dashed lines* show contributions of the two populations under conditions of independent engagement via the series spring (Eqs. 11 and 12; first-order Boltzmann functions with sensitivity values Z_1 and Z_2 as obtained from fits)

K_1=0.24±0.16 and K_2=4.7±0.9. For VHCs, K_1 was found to be essentially zero, while K_2=3.9±1.5. The combination of K_1<1 and K_2>1, as found for both OHCs and VHCs and other hair cell types, leads to a mere superposition (Figs. 2 and 3, red curves) of activity of two only slightly interdependent channels (Figs. 2 and 3, solid green and blue curves). Interdependency between the channels is small but consistently observed at hair bundle positions around X=0, where especially the less sensitive channel's activation (blue curves) deviates somewhat from the symmetric first-order Boltzmann relationships (Figs. 2 and 3, dashed green and blue curves calculated with Eqs. 11 and 12), which would have been expected if interdependency were completely absent (see "Materials and methods" section).

Series engagement was considered previously and was suspected to lead to interdependency between the channels termed negative cooperativity [15]. Negative cooperativity would result in a poorer displacement sensitivity compared to that obtained with independently activated transducer channels and was considered an unlikely mechanism of hair cell transduction (reviewed in [7]). We find here, however, that series engagement of two channels on either side of a tip link provides an accurate description of transduction while allowing for almost no interdependent, but instead, complementary activation without loss of sensitivity.

Negative cooperativity

We found that the model could also produce strong interdependency resulting in negative cooperativity of two channels if they possessed different sensitivities ($Z_1 \neq Z_2$), and under the condition that both $K_1 \gg 1$ and $K_2 \gg 1$ (Fig. 4). Then, the most sensitive channel (solid green line), when opened by increased bundle deflection, induces closure of the less sensitive channel (negative slope of solid blue curve) via a concurrent release in the gating spring tension. The sensitivity of overall activation (Fig. 4, red curve) is then reduced as a consequence and is smaller than the sensitivity of each of the channels when independently engaged (Fig. 4, dashed green and blue curve). Contrary to this theoretically possible mode of series engagement that would compromise the overall sensitivity of transduction, our results from fitting the model to measured transducer currents of mouse OHCs and VHCs clearly indicate a different regime, in which the two channels in series are complementarily recruited, so that their intrinsic sensitivities are effectively additive in the overall activation curve (Fig. 2). Results on auditory hair cells from the turtle and the rat, as well as saccular hair cells of the frog, show a similar lack of negative cooperativity when fitted with the series engagement model (Fig. 3).

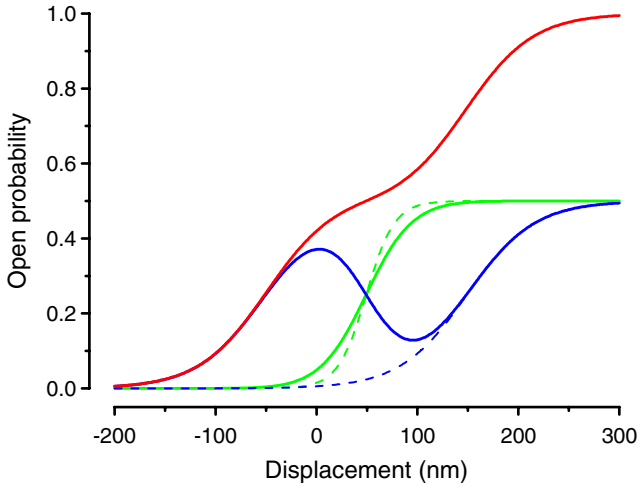

Fig. 4 Theoretical interdependency of two transducer channels engaged in series by a single tip link. Calculated open probability of a pair of channels (*p*, *red*) together with the partial contributions of the sensitive channel ($p_1/2$, *green*) and the less sensitive channel ($p_2/2$, *blue*). Negative cooperativity results if both K_1 and K_2 are significantly larger than 1 (i.e., unlike the results found for OHCs and VHCs and other hair cell types), so that less sensitive channels are closed with increasing hair bundle displacement in a certain range (*negative slope of blue trace*). As a consequence, the overall open probability has a plateau around p=0.5 with reduced sensitivity. *Dashed curves* give the partial contribution of the two channels if independently engaged (calculated with Eqs. 11 and 12; *dashed green curve* was shifted to have it centered with *solid green curve* to facilitate comparison). The effective sensitivity of the most sensitive channel is also reduced by the interaction. Sensitivities and set point are chosen to equal the mean parameters found for mouse OHCs: Z_1= 386 fN; Z_2=162 fN; X_0=49 nm, while K_1=20 and K_2=20

Effects of depolarization

An interesting feature of the series engagement model is that it may explain changes of activation curves as observed under depolarized potentials in terms of a differential effect on the two channel populations. The main effect observed upon depolarization is a negative shift of the lower part of *I–X* activation curves along the displacement axis resulting in a reduction of the asymmetry of the activation curve [21, 22], as also illustrated in Fig. 5 for a mouse OHC depolarized from −84 to + 86 mV. In terms of the present series engagement model, the effect can almost exclusively be attributed to a change of the most sensitive hair cell population (1). In addition to a reduction of about 20% of its sensitivity (Fig. 5, Z_1=286 fN (−84 mV); Z_1=226 (+86 mV)), the most prominent change is a negative shift of X_{01} of about 39 nm (mean shift, ΔX_{01}=25 nm, n=4) of the most sensitive population (Fig. 5, X_{01}=27 nm (−84 mV); X_{01}=−12 nm (+86 mV)). Shifts in X_{01} and X_{02} are governed in the present model by a change in the interaction parameter K_2 and the set point X_0 (Eqs. 11 and 12). To determine the underlying changes of the physical parameters,

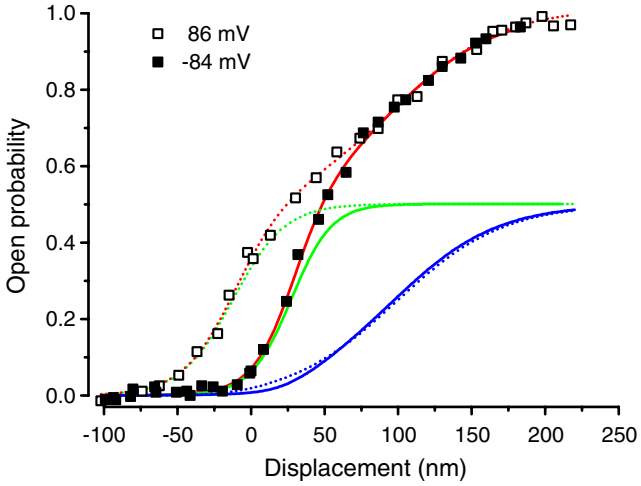

Fig. 5 Effects of depolarization on transducer channel open probability of a mouse OHC, compared with the series engagement model. *Red curves* show model responses (Eq. 4) fitted to the total open probability, while the *green and blue curves* depict individual contributions of the two populations of channels (Eqs. 5–8). *Filled squares* present results for a holding potential of −84 mV and *solid lines* fitted results to these data with parameters Z_1=286 fN; Z_2=116 fN; X_0=49 nm; K_1=0.04; K_2=3.98. *Open squares* present data for a holding potential of +86 mV and *dotted lines* fitted these data with parameters Z_1=226 fN; Z_2=115 fN; X_0=26 nm; K_1=0; K_2=7.93. G_T was 4.7 nS at −84 mV and 4.6 nS at +86 mV

we may first use Eq. (14) and the observation that X_{02} (Fig. 5, X_{02}=97 nm (−84 mV); X_{02}=99 nm (+86 mV)) and Z_2 (Fig. 5, Z_2=116 fN (−84 mV); Z_2=115 fN (+86 mV)) are virtually unchanged, so it may be concluded that X_e also remains unchanged by depolarization. Neglecting the change in Z_1, the shift in X_{01} (Eq. 13) can be merely attributed to a change in the energy difference between closed and open state of population (1) (μ_{CO}–μ_{OO}). Then, using Eq. (13), the extra energy required to open the (unengaged) channel under hyperpolarized (−84 mV) rather than depolarized (+86 mV) conditions can be estimated to amount to about $Z_1 \cdot \Delta X_{01} \cong 1.3kT$.

Discussion

The proposed series engagement of two channels by a single tip link provides a powerful model that quantitatively explains mechano-electrical transducer conductance measured in variety of hair cell types ranging from mammalian inner, outer, and vestibular hair cells (Figs. 2a, b, 3c and d) as well as turtle auditory (Fig. 3a) and frog saccular hair cells (Fig. 3b). For comparison, we have also tested the quality of fits of two alternative models, i.e., the three-state conformational model [cf. 5, 6] and a model consisting of a pure sum of two single Boltzmann activation curves to describe our data set [20]. The second alternative model is motivated by the observation that tip links may split into two strands that each may independently activate a single channel [14], and is equivalent to the present series engagement model under the condition $K_1 \cdot K_2 = 1$ (Eqs. 11 and 12). We found that both alternative models also produce very adequate fits as judged by their mean R^2 (independent double channel model, R^2=0.99701; three-state conformational model, R^2=0.99707) in comparison to the present series engagement model (R^2=0.99709). The latter model, however, is the only one in line with high-resolution calcium imaging studies indicating that a single tip link engages two channels on either side of it [15] which is further supported by recent detailed studies of transducer currents in cochlear outer and inner hair cells [17], which provide strong evidence for two operational transducer channels for every tip link.

Consequences of proposed model

The series engagement scheme offers some additional supportive inferences and interesting consequences.

First, series engagement provides a more parsimonious two-conformational-state channel description than the more complex three-conformational-state channel models previously used to describe the asymmetries of hair cell activation curves [5, 6, 17, 20–21, 23–27]. These asymmetries are found in a variety of different hair cell types and by using different stimulus techniques, such as stiff and compliant probes to directly move a hair bundle as well as hydrodynamic stimuli produced by micro fluid jets. The asymmetries depend on the membrane potential ([21, 22], cf. "Results" section) and extracellular Ca^{2+} [27, 28] and are therefore most likely an intrinsic feature of the transduction process.

Second, although the preceding analysis does not provide direct information on which end of the tip links the two channel populations are located, their contributions to the total transducer conductance can be separated and associated with their effective swing distances (d_1, d_2). Because the channels are mechanically coupled in series, the resulting gating spring constant (k_s) is the same for both channels, so that the ratio of their gating forces, or displacement sensitivities, must equal the ratio of their effective conformational swing distances (i.e., $Z_1/Z_2 = (K_sD_1)/(K_sD_2) = d_2/d_1$). Our results show that this ratio is 0.44±0.06 for OHCs and 0.66±0.11 for VHCs. From the single fits to the other hair cell types (Fig. 3), we find 0.42 for turtle auditory hair cells as well as rat inner and outer hair cells and 0.23 for frog saccular hair cells. Assuming the two channel populations to have identical conformational swings, these ratio values may be geometrically interpreted by considering that the directions of these channel swings have different angles with the direction of the tip link along which

the forces are applied to the gates. Effective distances of the conformational swing (d_1, d_2) then derive from their projections on the direction of the tip links. An interesting hypothesis is that the channels' orientations are as suggested in Fig. 1b and c, where the upper channel's conformational swing is more in line with the tip link than that of the lower channel, so that the most sensitive channel population would be on the side of the taller stereocilium, and the less sensitive channel population at the tip of the shorter stereocilium.

The differences found in absolute displacement sensitivities (Z_1, Z_2) for different hair cell types may thus reflect differences in orientation between tip link and channel swing but also differences in the geometry of the hair bundles, especially the diameter–length ratio of individual stereocilia [4]. The ratio of the displacement sensitivity between mouse OHCs and VHCs has been estimated previously to be about two, similar to what is found in this study (range 2.6–1.6) and interpreted as an equal sensitivity in terms of hair bundle rotation, if the approximate length ratio of a factor of two is taken into account [20].

Recently, it was reported that the tip link's composition is asymmetrical, consisting of a cadherin 23 dimer spanning the upper two thirds of its length and a protocadherin 15 dimer forming the lower third [11]. This at least hints at an asymmetry in the physical nature of the coupling of the tip link's ends to the two companion channels and may be related to different orientations of the channels with respect to the tip link's direction.

Intrinsic differences in the channels and their properties leading to different values for d_1 and d_2 can certainly not be excluded. A clear difference between the two channel populations, as described by the present model, is found with respect to their responses to depolarization. Apparently, only the most sensitive channel population is affected, most significantly via a change in its (unengaged) conformational energies but also via a reduction in sensitivity of about 20% (Fig. 5). It is generally assumed that depolarization affects Ca^{2+}-dependent adaptation processes like calcium binding to the channel (fast adaptation) or the action of actin–myosin motor molecules (slow adaptation), resetting the resting tension in tip links and gating springs [22, 29]. The present results (Fig. 5) thus suggest that the observed changes of activation curves upon depolarization may be related to the fast adaptation process modulating conformational energies with an amount of the order of kT via a voltage dependent effect on Ca^{2+}.

In the derivation of the activation curve, there was no extra parameter introduced to account for a possible asymmetry in conductance between the populations (Eq. 4). Although we cannot exclude a conductance difference, the quality of the fits to the measured data did not justify the introduction of an extra model parameter at this stage using the available data.

Third, an interesting consequence of the present model is that transducer activation of hair cells with only one remaining operational transducer channel are expected to follow symmetric first-order Boltzmann kinetics, while recordings of the intact hair cell show asymmetric activation curves. Although single transducer channel data are scarce, complete activation curves have indeed been reported and were adequately fit by first-order Boltzmann curves [16, 17]. Assuming the present model, an inherent difficulty of obtaining single channel data in hair cells may be related to the special conditions required, in which one channel of a pair is intact while its companion channel is still mechanically coupled but not responsive. More direct tests of the validity of the present model may need to involve stimulation of a single tip link, or selective activation of a single channel on either side of a tip link, for instance by using laser tweezers (optical trap) [30] or atomic force microscopy [31].

Lastly, we find that series engagement produces input–output characteristics of transduction that are appropriate for sensitive coding at low displacement levels by one channel population and more compressive coding at higher levels by the other population, thereby linking auditory sensitivity and dynamic range. Similarly shaped input–output characteristics have been observed in the visual system, and have been shown to optimize information capacity since they represent the cumulative probability function for stimulus intensities [32, 33]. Adaptive strategies to match the input–output characteristics to external stimulus conditions in order to enhance information transmission have been identified as a key feature in biological sensory systems [34]. The same concept of achieving biphasic asymmetric input–output functions by combining a sensitive detector unit with a second more compressive one has recently been utilized in digital camera image sensors to resolve more detail in highlight and dark areas of an image [35].

Conclusions

In summary, a large set of experimental data is compatible with a mechanical model of mechano-electrical transduction where two channels are activated via a single connecting tip link. Interdependency between the two channel populations is small, representing two dual-state channels, each with its specific sensitivity and set point. This straightforward interpretation provides a new framework for understanding the kinetics of hair cell transduction and merits further exploration and comparison to other models of activation.

Acknowledgements A.B.A. Kroese, P. Pirih, and D.G. Stavenga commented on previous versions of the manuscript. This work has been partially supported by the Netherlands Organization for Scientific Research (SvN, CJWM) and the Medical Research Council (CJK, GWTL, CJWM).

References

1. Hudspeth AJ (1989) How the ear's works work. Nature 341:397–404
2. Fettiplace R, Hackney CM (2006) The sensory and motor roles of auditory hair cells. Nat Rev Neurosci 7:19–29
3. Gillespie PG, Dumont RA, Kachar B (2005) Have we found the tip link, transduction channel, and gating spring of the hair cell. Curr Opin Neurobiol 15:389–396
4. Howard J, Hudspeth AJ (1988) Compliance of the hair bundle associated with gating of mechanoelectrical transduction channels in the bullfrog's saccular hair cell. Neuron 1:189–199
5. Corey DP, Hudspeth AJ (1983) Kinetics of the receptor current in bullfrog saccular hair cells. J Neurosci 3:962–976
6. Markin VS, Hudspeth AJ (1995) Gating spring models of mechanoelectrical transduction by hair cells of the inner ear. Annu Rev Biophys Biomol Struct 24:59–83
7. Bechstedt S, Howard J (2007) Models of hair cell mechanotransduction. In: Hamill O, Simon S, Benos D (eds) Current topics in membranes, vol 59. Elsevier, Amsterdam
8. Lumpkin EA, Hudspeth AJ (1995) Detection of Ca^{2+} entry through mechanosensitive channels localizes the site of mechanoelectrical transduction in hair cells. Proc Natl Acad Sci USA 92:10297–10301
9. Jaramillo F, Hudspeth AJ (1991) Localization of the hair cell's transduction channels of the hair bundle's top by iontophoretic application of a channel blocker. Neuron 7:409–420
10. Pickles JO, Comis SD, Osborne MP (1984) Cross-links between stereocilia in the guinea pig organ of Corti, and their possible relation to sensory transduction. Hearing Res 15:103–112
11. Kazmierczak P, Sakaguchi H, Tokita J et al (2007) Cadherin 23 and protocadherin 15 interact to form tip-link filaments in sensory hair cells. Nature 499:87–92
12. Zhao Y, Yamoah EN, Gillespie GP (1996) Regeneration of broken tip links and restoration of mechanical transduction in hair cells. Proc Natl Acad Sci USA 93:15469–15474
13. Hudspeth AJ, Corey DP (1977) Sensitivity, polarity and conductance change in the response of vertebrate hair cells to controlled mechanical stimuli. Proc Natl Acad Sci USA 74:2407–2411
14. Kachar B, Parakkal M, Kurc M et al (2000) High-resolution structure of hair-cell tip links. Proc Natl Acad Sci USA 97:13336–13341
15. Denk W, Holt JR, Shepherd GMG, Corey DP (1995) Calcium imaging of single stereocilia in hair cells: localization of transduction channels at both ends of tip links. Neuron 15:1311–1321
16. Ricci AJ, Crawford AC, Fettiplace R (2003) Tonotopic variation in the conductance of the hair cell mechanotransducer channel. Neuron 40:983–990
17. Beurg M, Evans MG, Hackney CM et al (2006) A large-conductance calcium-selective mechanotransducer channel in mammalian cochlear hair cells. J Neurosci 26:10992–11000
18. Holt JR, Gillespie SK, Provance DW et al (2002) A chemical-genetic strategy implicates myosin-1c in adaptation by hair cells. Cell 108:371–81
19. Kros CJ, Marcotti W, van Netten SM et al (2002) Reduced climbing and increased slipping adaptation in cochlear hair cells of mice with Myo7a mutations. Nat Neurosci 5:41–47
20. Geleoc GS, Lennan GW, Richardson GP et al (1997) A quantitative comparison of mechanoelectrical transduction in vestibular and auditory hair cells of neonatal mice. Proc Roy Soc Biol Sci 264:611–621
21. Crawford AC, Evans MG, Fettiplace R (1989) Activation and adaptation of transducer currents in turtle hair cells. J Physiol 419:405–434
22. Assad JA, Hacohen N, Corey DP (1989) Voltage dependence of adaptation and active bundle movement in bullfrog saccular hair cells. Proc Natl Acad Sci USA 86:2918–2922
23. Shepherd GMG, Corey DP (1994) The extent of adaptation in bullfrog saccular hair cells. J Neurosci 14:6617–6229
24. Holton T, Hudspeth AJ (1986) The transduction channel of hair cells from the bull-frog characterized by noise analysis. J Physiol 375:195–227
25. Kros CJ, Rüsch A, Richardson GP (1992) Mechano-electrical transducer currents in hair cells of cultured neonatal mouse cochlea. Proc Roy Soc Biol Sci 259:185–193
26. van Netten SM, Kros CJ (2000) Gating energies and forces of the mammalian hair cell transducer channel and related hair bundle mechanics. Proc Roy Soc Biol Sci 267:1915–1923
27. Crawford AC Evans MG, Fettiplace R (1991) The actions of calcium on the mechano-electrical transducer current of turtle hair cells. J Physiol 434:369–398
28. Assad JA, Corey DP (1992) An active motor model for adaptation by vertebrate hair cells. J Neurosci 12:3291–3309
29. Ricci AJ, Crawford AC, Fettiplace R (2002) Mechanisms of active hair bundle motion in auditory hair cells. J Neurosci 22: 44–52
30. Cheung EL, Corey DP (2005) Ca^{2+} changes the force sensitivity of the hair-cell transduction channel. Biophys J 90:124–139
31. Langer MG, Fink S, Koitschev A et al (2001) Lateral mechanical coupling of stereocilia in cochlear hair bundles. Biophys J 80:2608–2621
32. Laughlin SB (1981) A simple coding procedure enhances a neuron's information capacity. Z Naturforsch 36c:910–912
33. Laughlin SB (1983) Matching codes to scenes to enhance efficiency. In: Braddick OJ, Sleigh AC (eds) Physical and biological processing of images. Springer, New York
34. Brenner N, Bialek W, de Ruyter van Steveninck R (2000) Adaptive rescaling maximizes information transmission. Neuron 26:695–702
35. Ashida T, Yamashita H, Yoshida M et al (2004) Signal processing and automatic camera control for digital still cameras equipped with a new type CCD. In: Blouke MM, Sampat N, Motta RJ (eds) Sensors and camera systems for scientific, industrial, and digital photography, Applications V, Proc SPIE Int Soc Opt Eng 5301